

Mapping NGC 7027 in New Light: CO⁺ and HCO⁺ Emission Reveal Its Photon- and X-ray-Dominated Regions

JESSE BUBLITZ,^{1,2} JOEL H. KASTNER,² PIERRE HILY-BLANT,³ THIERRY FORVEILLE,³ MIGUEL SANTANDER-GARCÍA,⁴
JAVIER ALCOLEA,⁴ VALENTIN BUJARRABAL,⁴ DAVID J. WILNER,⁵ RODOLFO MONTEZ, JR.,⁵ AND ISABEL ALEMAN⁶

¹Green Bank Observatory, 155 Observatory Road, Green Bank, WV 24944, USA

²Chester F. Carlson Center for Imaging Science and Laboratory for Multiwavelength Astrophysics, Rochester Institute of Technology, 54 Lomb Memorial Drive, Rochester, NY 14623, USA

³Université Grenoble Alpes, CNRS, IPAG, F-38000 Grenoble, France

⁴Observatorio Astronómico Nacional, Alfonso XII, 3, 28014, Madrid, Spain

⁵Harvard-Smithsonian Center for Astrophysics, 60 Garden Street, Cambridge, MA 02138, USA

⁶UNIFEI, Instituto de Física e Química, Universidade Federal de Itajubá, Av. BPS 1303 Pinheirinho, 37500-903 Itajubá, MG, Brazil

(Received September 13, 2022; Revised November 16, 2022; Accepted November 18, 2022)

Submitted to ApJ

ABSTRACT

The young and well-studied planetary nebula NGC 7027 harbors significant molecular gas that is irradiated by luminous, point-like UV (central star) and diffuse (shocked nebular) X-ray emission. This nebula represents an excellent subject to investigate the molecular chemistry and physical conditions within photon- and X-ray-dominated regions (PDRs and XDRs). As yet, the exact formation routes of CO⁺ and HCO⁺ in PN environments remain uncertain. Here, we present $\sim 2''$ resolution maps of NGC 7027 in the irradiation tracers CO⁺ and HCO⁺, obtained with the IRAM NOEMA interferometer, along with SMA CO and HST 2.12 μm H₂ data for context. The CO⁺ map constitutes the first interferometric map of this molecular ion in any PN. Comparison of CO⁺ and HCO⁺ maps reveal strikingly different emission morphologies, as well as a systematic spatial displacement between the two molecules; the regions of brightest HCO⁺, found along the central waist of the nebula, are radially offset by $\sim 1''$ (~ 900 au) outside the corresponding CO⁺ emission peaks. The CO⁺ emission furthermore precisely traces the inner boundaries of the nebula's PDR (as delineated by near-IR H₂ emission), suggesting that central star UV emission drives CO⁺ formation. The displacement of HCO⁺ radially outward with respect to CO⁺ is indicative that dust-penetrating soft X-rays are responsible for enhancing the HCO⁺ abundance in the surrounding molecular envelope, forming an XDR. These interferometric CO⁺ and HCO⁺ observations of NGC 7027 thus clearly establish the spatial distinction between the PDR and XDR formed (respectively) by intense UV and X-ray irradiation of molecular gas.

Keywords: Planetary Nebulae(1249) — Bipolar Nebulae(155) — Astrochemistry(75) — Molecular Gas(1073) — Radio Astronomy(1338)

1. INTRODUCTION

As a nearby ($D \sim 890$ pc; Masson 1989; Ali et al. 2015), young (dynamical age ~ 1000 yrs; Ali et al. 2015; Schönberner et al. 2018) and rapidly evolving planetary nebula (PN) with a massive molecular envelope, NGC 7027 represents an excellent source to study the effects of UV and X-ray-induced chemical processes in molecular gas. Photometric studies have identified a hot central star of $T_{eff} \sim 200$ kK that drives photoionization

and photodissociation in the ejected envelope (Graham et al. 1993; Latter et al. 2000; Zhang et al. 2005; Moraga et al. 2022). The central star (CSPN) of NGC 7027 is a luminous extreme UV source ($L_{UV} \sim 3 \times 10^{37}$ ergs s⁻¹; Latter et al. 2000; Moraga et al. 2022), while Chandra X-ray Observatory observations established NGC 7027 as among the most luminous, diffuse X-ray sources among PNe, with a luminosity of $L_X = 7 \times 10^{31}$ ergs s⁻¹ (Kastner et al. 2012; Montez & Kastner 2018). Optical and IR

observations indicate a carbon-rich nebula ($C/O = 2.7$; Zhang et al. 2005), which is consistent with detections of C- and O-based species in the molecular envelope, suggesting a progenitor mass of 2–4 M_{\odot} (Kastner & Wilson 2021, and references therein). The temperature and luminosity of NGC 7027’s CSPN indicate a present-day mass of $\sim 0.7 M_{\odot}$ (Moraga et al. 2022).

NGC 7027 yielded the first identification of a molecule in any PN (CO; Mufson et al. 1975) and now boasts one of the largest catalogs of molecular transitions detected in a single PN. The nebula is particularly rich in emission from molecular ions, including detections of HCO^+ , CO^+ , and N_2H^+ (Deguchi et al. 1990; Zhang et al. 2008), and the first-ever astrophysical detection of HeH^+ (Güsten et al. 2019). Radio interferometric maps of NGC 7027 in emission from HCO^+ (Deguchi et al. 1992; Likkell 1992; Huang et al. 2010), CO (Biegging et al. 1991; Fong et al. 2006), and ^{13}CO (Nakashima et al. 2010) have previously been obtained, typically at 2–4'' resolution. A recent, comprehensive HST imaging study from near-UV to near-IR (Figure 1) provides additional detail concerning this collimated outflow system, including evidence for strong shocks along one of the three main outflow axes (Moraga et al. 2022). However, since the aforementioned interferometric observations, made between 2008 and 2010 (Zhang et al. 2008; Huang et al. 2010; Nakashima et al. 2010), no radio-based mapping of NGC 7027 has been published.

NGC 7027 also constitutes a well-studied example of UV-excited fluorescent emission from molecular hydrogen, which arises from within a photodissociation (or photon-dominated) region (PDR) along the inner boundary of its massive molecular envelope (Graham et al. 1993). Latter et al. (2000) established the detailed structure of this hot H_2 -emitting region via near-IR imaging with the Hubble Space Telescope. Followup ground-based near-IR imaging spectroscopy of H_2 was interpreted as revealing multiple collimated outflows scattered over a wide range of outflow axes (Cox et al. 2002), providing the basis for the multipolar outflow model later proposed by Nakashima et al. (2010).

In this paper, we present interferometric mapping of NGC 7027 in two highly reactive molecular ions, CO^+ and HCO^+ . These two molecules are particularly interesting for purposes of understanding the structures and molecular chemistries of PDRs as well as X-ray-dominated regions (XDRs). However, present theory leaves open the precise mechanisms whereby CO^+ and HCO^+ might trace PDR versus XDR chemical processes, and how the two molecules might act more generally as probes of non-LTE chemistry in astrophysical sources. This uncertainty serves as the prime motiva-

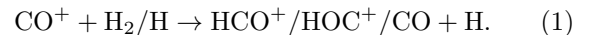
tion for our comparative observational study of CO^+ and HCO^+ emission from NGC 7027.

Enhanced abundances of CO^+ are likely found exclusively in such regions of high far-UV or X-ray flux. In (O-rich) ISM PDRs, CO^+ can be formed via reactions between OH and C^+ (Latter et al. 1993), where the C^+ is generated via photodissociation and then ionization of CO. If so, then CO^+ should primarily reside along PDR transition layers, between fully atomic and fully molecular gas.

The sole empirical observation that supports such a connection between CO^+ and dense PDR environments is a single-dish map of CO^+ emission within the star-forming region Mon R2 (Treviño-Morales et al. 2016). These observations established that CO^+ is cospatial with the PAH and [C II] emission found at the H_I/H_2 interface, as expected.

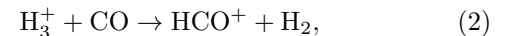
However, in the case of irradiation of molecular gas by photons with energies > 14 eV, CO can also directly form CO^+ . Furthermore, Spaans & Meijerink (2007) have shown that significant X-ray flux will boost CO^+ abundance through enhanced production of C^+ and OH. Because X-rays penetrate higher column densities of molecular gas more readily than UV photons, X-ray irradiation should enable CO^+ production beyond the reach of PDRs, i.e., within the surrounding XDRs.

Primary destruction paths of CO^+ consist of dissociative recombination as well as reactions with H_2 or with neutral H at intermediate depths (e.g., Stäuber & Bruderer 2009). One of the possible CO^+ destruction products is HCO^+ , via the reaction



Modeling by Bell et al. (2007) shows CO^+ line intensity to increase weakly in conjunction with that of HCO^+ , but were unable to draw conclusions as to whether the presence of CO^+ leads to HCO^+ enhancement. If such were the case, one would expect to see cospatial HCO^+ and CO^+ emission.

Alternatively, HCO^+ will form at large depths in X-ray-irradiated molecular gas via



where H_3^+ abundance enhancement is due to X-ray ionization of H_2 (e.g., Deguchi et al. 1990). Models of gaseous nebulae have indeed shown that the strong X-ray irradiation characteristic of XDRs is required to produce observed column densities of HCO^+ (Kimura et al. 2012). In contrast, photodissociative recombination of H_3^+ with electrons should limit HCO^+ production in PDR environments.

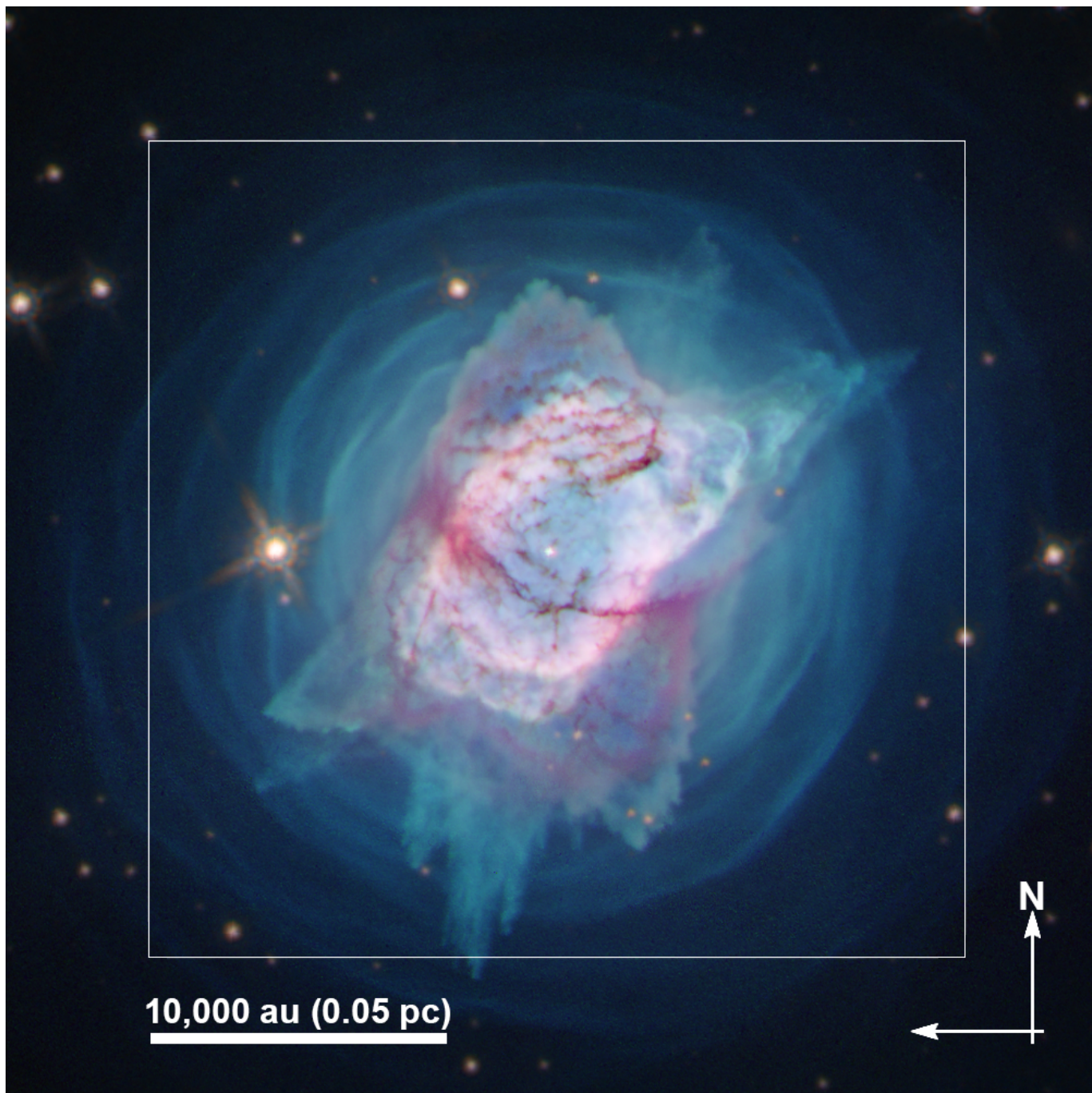


Figure 1. Composite image of NGC 7027 from HST/WFC3 using wide IR (red: F110W, blue: F160W) and narrow band (red: F128N+F130N, green: F673N+F656N, blue: F502N+F342N+F487N) filters. Field of view is $40'' \times 40''$. The white box marks the $30'' \times 30''$ field of view of other figures in this work. N is up, E is to the left. Image credit: STScI.

The foregoing implies that direct comparison of the CO^+ and HCO^+ spatial distributions in planetary nebulae should provide a straightforward test of XDR- vs PDR-like chemistry. Specifically, if FUV/EUV photons dominate CO^+ production, in a PDR (through $\text{C}^+ + \text{OH}$), then one expects CO^+ to trace the C^+ layer (as in Mon R2; Treviño-Morales et al. 2016), which should in turn coincide with a region of fluorescent

(near-IR) H_2 emission (Graham et al. 1993). HCO^+ would then either be found in an XDR in the surrounding molecular envelope, where $\text{CO} + \text{H}_3^+$ becomes an efficient HCO^+ production mechanism, or in the PDR, if dissociative recombination of CO^+ drives HCO^+ production. A third possibility is that CO^+ and HCO^+ both derive from CO , through direct X-ray ionization and via collisions with H_3^+ , respectively; in this case the

two species would also be expected to coincide spatially, but in an XDR that surrounds the PDR traced by near-IR H_2 .

To date, HCO^+ has been detected in a few dozen planetary nebulae (e.g., Schmidt & Ziurys 2016, 2017; Bublitz et al. 2019), and (as noted) has been mapped in NGC 7027, while CO^+ emission has been identified in seven PNe (Latter et al. 1993; Bell et al. 2007). However, the detailed spatial distribution of the latter molecule remains to be established in any PN. To fill this void, we have conducted an interferometric mapping study of NGC 7027 in CO^+ $J = 2 \rightarrow 1$ and HCO^+ $J = 1 \rightarrow 0$ emission with the Institut de Radioastronomie Millimétrique’s (IRAM) NOrthern Extended Millimeter Array (NOEMA).

In Section 2, we describe the NOEMA and supplementary (archival) observations. The results, including CO^+ and HCO^+ velocity channel maps and velocity-integrated images, are presented in Section 3. Section 4 presents an analysis of the structures of the CO^+ and HCO^+ emitting regions in NGC 7027, including a comparison with each other and with archival CO and H_2 imaging, in addition to new evidence of the nebula’s multi-polar jet system as traced by HCO^+ emission. Conclusions are presented in Section 5.

2. OBSERVATIONS

2.1. NOEMA Data

Observations of NGC 7027 were carried out at the $J = 2 \rightarrow 1$ rotational transition of CO^+ (235.380 GHz) and the $J = 1 \rightarrow 0$ transition of HCO^+ (89.189 GHz) and adjacent continuum with the Northern Extended Millimeter Array (NOEMA) interferometer in 2017 March–May and 2018 April, respectively. A phase center of the nebula R.A.(2000.0) = $21^{\text{h}}07^{\text{m}}01^{\text{s}}.8$, dec.(2000.0) = $42^{\circ}14'10''$ was chosen for the CSPN (Huang et al. 2010). All NOEMA antennae are equipped with dual polarization, heterodyne receivers that provide a bandwidth of 7.722 GHz across the lower and upper sidebands. The wide-band correlator WideX was configured for a contiguous bandwidth of 3.6 GHz and channel spacings of 1.95 MHz, for a velocity resolution of 2.48 km s^{-1} at the CO^+ line. Eight antennae were used in the most compact configuration D and an on-source time of 9.6 hours. Baselines ranged from 24–176 m, with an angular resolution of $1''.51 \times 1''.42$ (P.A. = -74°) at 236 GHz and peak S/N in the continuum of ~ 24 .

The introduction in late 2017 of an additional antenna and the new wide-band PolyFiX correlator allowed us to achieve a velocity resolution of 0.5 km s^{-1} for the HCO^+ line. The survey observations were performed using nine antennae in the intermediate configuration C, for an on-

source time of 7.4 hours. Baselines of 24–704 m achieved an angular resolution of $2''.09 \times 2''.07$ (P.A. = 62°) for the 89.0 GHz HCO^+ line and peak S/N in the continuum of 36σ . A summary of observing details can be found in Table 1.

Table 1. NOEMA SPECTRAL LINE MAPPING OF NGC 7027: OBSERVATION SUMMARY

Molecule	CO^+	HCO^+
Frequency	235.380 GHz	89.189 GHz
Transition	$J = 2 \rightarrow 1$	$J = 1 \rightarrow 0$
Baselines	24–176 m	24–704 m
Beam Size	$1.51'' \times 1.42''$	$2.09'' \times 2.07''$
Spectral Resolution	1.95 MHz	0.149 MHz
Velocity Resolution	2.48 km s^{-1}	0.5 km s^{-1}
S/N for Continuum	24σ	36σ

Phase and amplitude calibrations utilized 2200+420, J2050+363, and J2120+445. Bandpass calibrations were performed with 3C84, 3C454.3, J2120+445, or 2013+370, with MWC349 for absolute flux calibration (1.08 Jy at 89 GHz, 1.94 Jy at 230 GHz). For the centered pointing, the phase center was used, while pointing and focusing errors of less than 30% were reported during observations. Typical seeing varied day-to-day, with an average of $0''.84$ for CO^+ and $0''.65$ for HCO^+ .

Data calibration was performed at the IRAM headquarters in Grenoble, France with the Continuum and Line Interferometer Calibration (CLIC) software package¹. A standard calibration script was followed for radiometric corrections, as well as phase, flux, and amplitude calibration to produce the UV tables. Continuum subtraction and self calibration were also performed, whereby strong continuum emission was used to calibrate the adjacent line data. Natural weighting was used to generate images from the visibilities, and then deconvolution was performed with the Hogbom clean algorithm. The resulting high-quality velocity channel maps of NGC 7027 in $\text{CO}^+(2-1)$ and $\text{HCO}^+(1-0)$ are presented in Figures 2 and 3, respectively; velocity-integrated (“moment 0”) $\text{CO}^+(2-1)$ and $\text{HCO}^+(1-0)$ images, as well as spectra extracted from the channel maps, are presented in Figure 4.

2.2. SMA and HST data

To place our NOEMA CO^+ and HCO^+ imaging results in context, we make use of (radio) CO and (near-

¹ <http://www.iram.fr/IRAMFR/GILDAS/>

IR) H₂ imaging obtained with the Submillimeter Array (SMA) and HST/NICMOS, respectively. SMA CO imaging of the nebula was obtained in the J=3→2 transition (345.796 GHz) on August 28, 2016 as part of a spectral line survey of NGC 7027 (Patel et al., in preparation). The array utilized the subcompact configuration, with baseline lengths of 9.5–69.1 m, and a synthesized beam size of 3''×2''. As such it should be noted that while the CO map adequately identifies the borders of the bulk of CO-rich gas in the nebula, it does not necessarily represent the total extent of CO. The observations were carried out in single pointing mode, with 15'' as the largest angular size of a continuous structure imaged by the subcompact array at this frequency. The phase center coordinates were R.A.(2000.0) = 21^h07^m01^s.5, dec.(2000.0) = 42°14'09.9'', while also used as the pointing center, and source velocity v_{LSR} of 25 km s⁻¹. All 8 antennae available at that time were operational, and the DSB T_{sys} values ranged from 400 to 600 K, varying between antennae and with source elevation. The zenith optical depth at 225 GHz was 0.1 throughout the track. The absolute flux calibration was determined by observations of Titan and Neptune. Complex visibility gain calibration was performed by observing BL Lac and MWC 349a periodically for 3 min each, between the observations of NGC 7027 for 12 min. The bright quasars 3C454.3 and 3C279 were observed for 1.5 hours each, for spectral bandpass calibration. The visibilities were calibrated using the MIR package in IDL². Imaging was performed using the *clean* task in CASA³. Continuum emission was subtracted prior to imaging the spectral line emission, using the *uvcontsub* task, identifying line-free channels in the u-v spectra by visual inspection. These data are among the first observations carried out with the SWARM correlator (Primiani et al. 2016), with a spectral resolution of 140 KHz per channel, which was smoothed by a factor of 8 to obtain higher S/N with a spectral resolution of ~0.97 km s⁻¹. The rms noise level in the imaged data cube is ~150 mJy/beam.

A map of 2.12 μm rovibrational emission from molecular hydrogen was generated from HST/NICMOS images available in the Hubble Legacy Archive (Project 7365, PI: William Latter; Latter et al. 2000). The 2.12 μm H₂ emission was isolated by appropriately weighting and subtracting images obtained using the NICMOS F190N and F215N filters from the F212N filter image,

² <https://lweb.cfa.harvard.edu/rtcd/SMAdata/process/overview/>

³ <https://casa.nrao.edu/>

to remove contaminating continuum and He I emission, respectively.

3. RESULTS

Figure 2 constitutes the first interferometric CO⁺ mapping of NGC 7027, or of any PN. Indeed, to our knowledge, this is only the second CO⁺ map obtained for any astrophysical source after that of the Mon R2 region (Treviño-Morales et al. 2016). Emission from the $N = 2 \rightarrow 1$ 236.1 GHz CO⁺ line spans roughly 1–48 km s⁻¹, with a central velocity of $V_{LSR} = 24.3$ km s⁻¹ (Figure 2), and a total CO⁺ flux of 391.2 Jy km s⁻¹. The nebula displays a multi-lobed structure in CO⁺, as seen most clearly near the systemic velocity and in the velocity-integrated moment 0 image (Figure 4). The channel maps demonstrate that, with the exception of the nebular waist (see below), the most blue-shifted CO⁺ is largely confined in the northeast regions of the nebula, while the most red-shifted CO⁺ is found in its southwest regions. As is discussed in more detail below, the overall CO⁺ emission morphology and kinematics, as revealed in both the channel maps (Figure 2) and the velocity-integrated image (Figure 4), are strikingly similar to those of near-IR (2.12 μm) H₂ emission (Cox et al. 2002, their Figures 5, 6). The brightest CO⁺ emission is detected along the waist or minor axis of the nebula (where the major axis is oriented along position angle $P.A. = -25^\circ$). Integrated over velocity (Figure 4), the CO⁺ emission is elliptical yet appears as an almond-shaped waist due to the view at an inclination of 35° (see also Cox et al. 2002).

Continuum emission in the vicinity of the CO⁺(2–1) line (mean frequency 236.5 GHz; Figure 5, top left) is well detected, and appears as an elliptical region whose major axis is well aligned with that of the velocity-integrated CO⁺ emission (i.e., $P.A. \sim -30^\circ$). The peak continuum emission is seen along the waist (minor axis) of the nebula, and there is a prominent gap or hole in the elliptical emitting region ~4–5'' northwest of the ellipse’s center (i.e., the position of the central star). The dimensions of the 1.3 mm continuum emission are 11.6''×9.1'', consistent with previous mm-wave mapping studies (e.g., Huang et al. 2010, and references therein).

The 89.6 GHz HCO⁺(1–0) line has here been mapped by NOEMA at an unmatched ~2'' resolution (Figures 3, 4). In Figure 3, the native PolyFiX correlator channel resolution of ~0.5 km s⁻¹ has been rebinned to 2.5 km s⁻¹ to match that of CO⁺(2–1). The HCO⁺ emission is observed to span a total velocity width of 47.5 km s⁻¹, with a central velocity of $V_{LSR} = 24.8$ km s⁻¹. We measure a total HCO⁺(1–0) flux of 1970 Jy km s⁻¹. Emission from HCO⁺ appears as an extended, evacu-

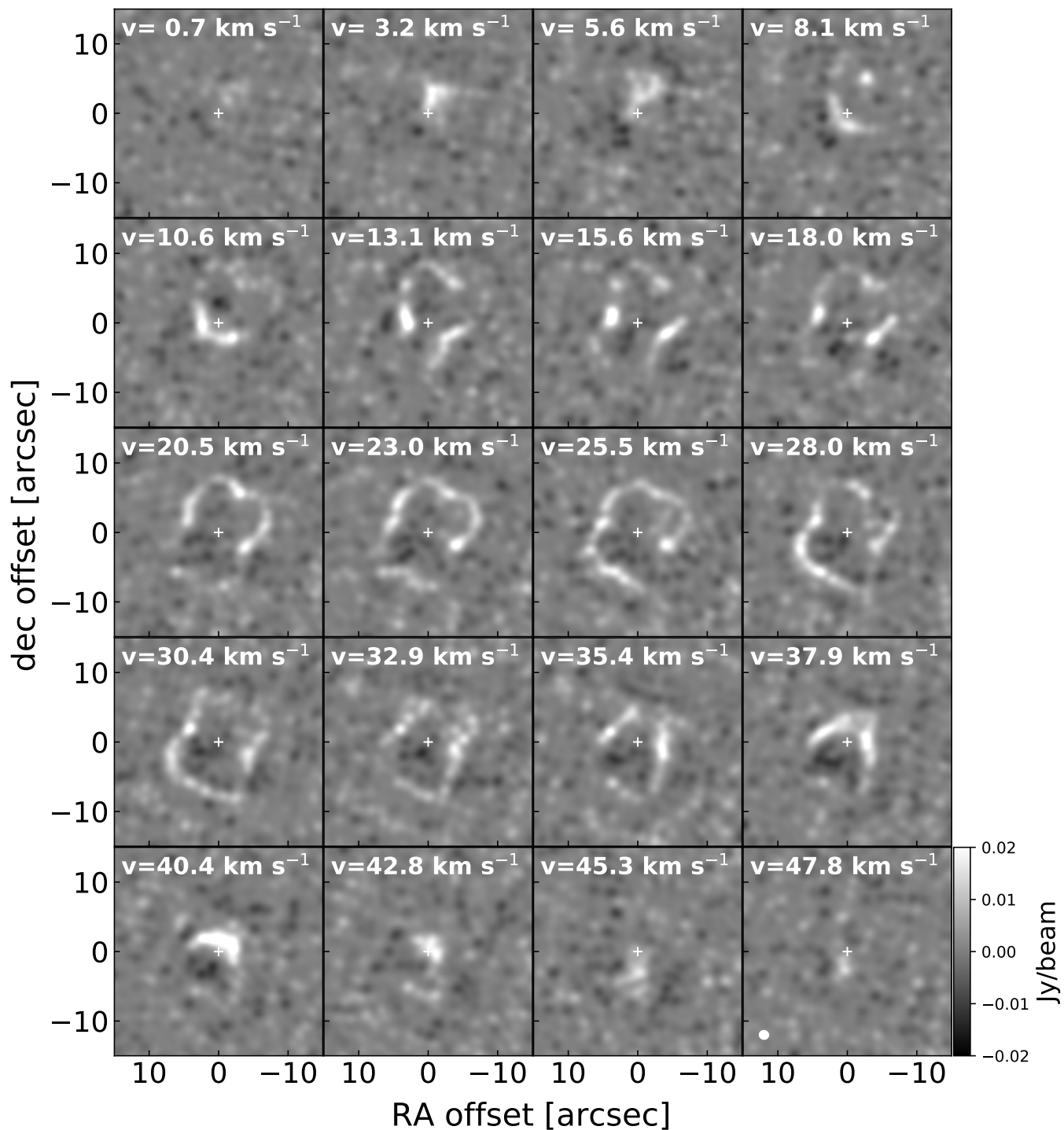


Figure 2. NOEMA channel maps of CO⁺(2-1) emission from NGC 7027, displayed at $\sim 2.5 \text{ km s}^{-1}$ intervals. Flux intensity scale is at lower right. Channel LSR velocity is indicated in each frame. The beam size is indicated by the white oval in the lower right frame and crosses indicates the position of the central star.

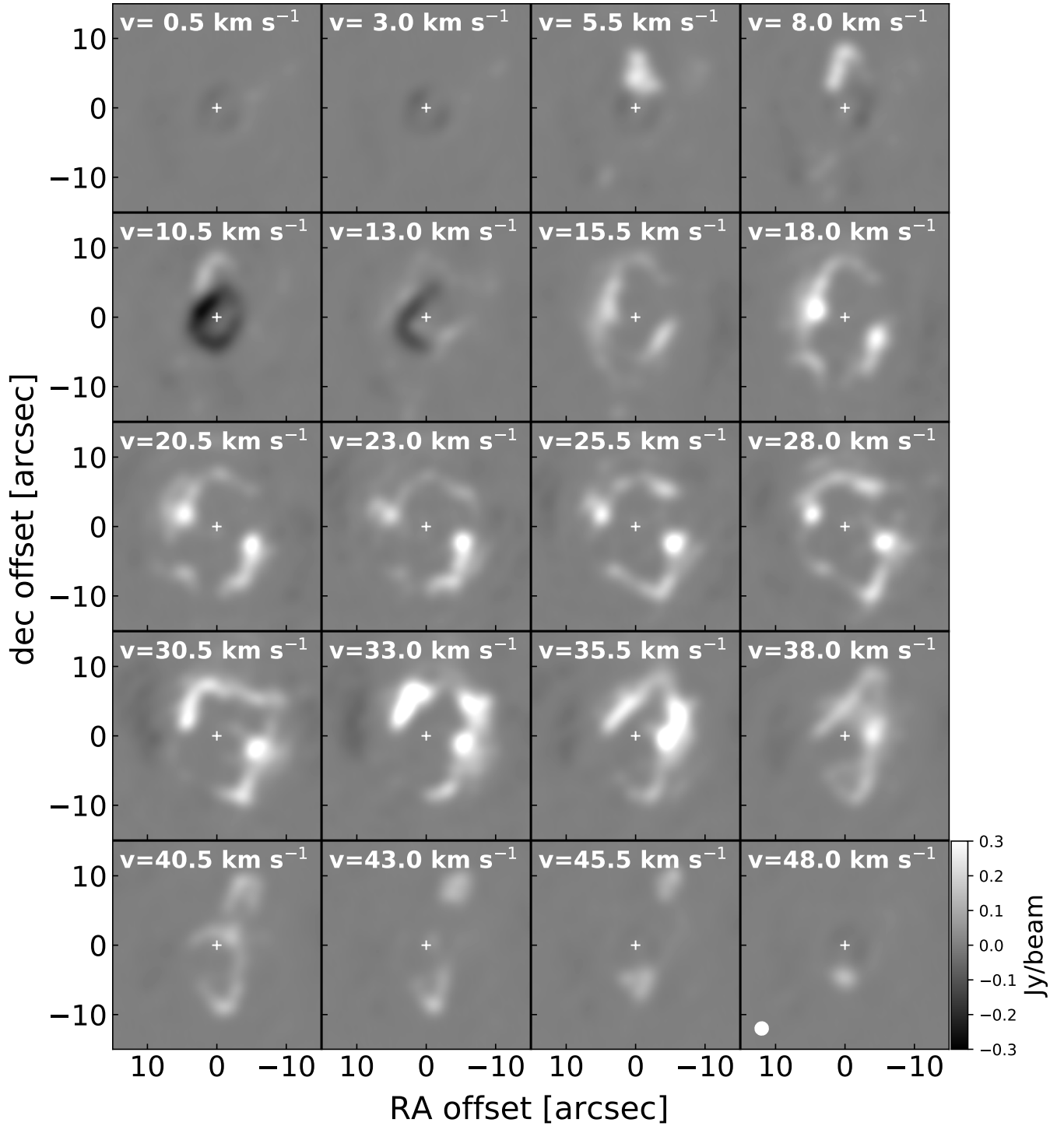


Figure 3. NOEMA channel maps of $\text{HCO}^+(1-0)$ emission from NGC 7027, presented at the same (2.5 km s^{-1}) velocity intervals as for $\text{CO}^+(2-1)$ (Figure 2). Flux intensity scale is at lower right. Channel LSR velocity is indicated in each frame. The beam size is indicated by the white oval in the lower right frame and crosses indicates the position of the central star.

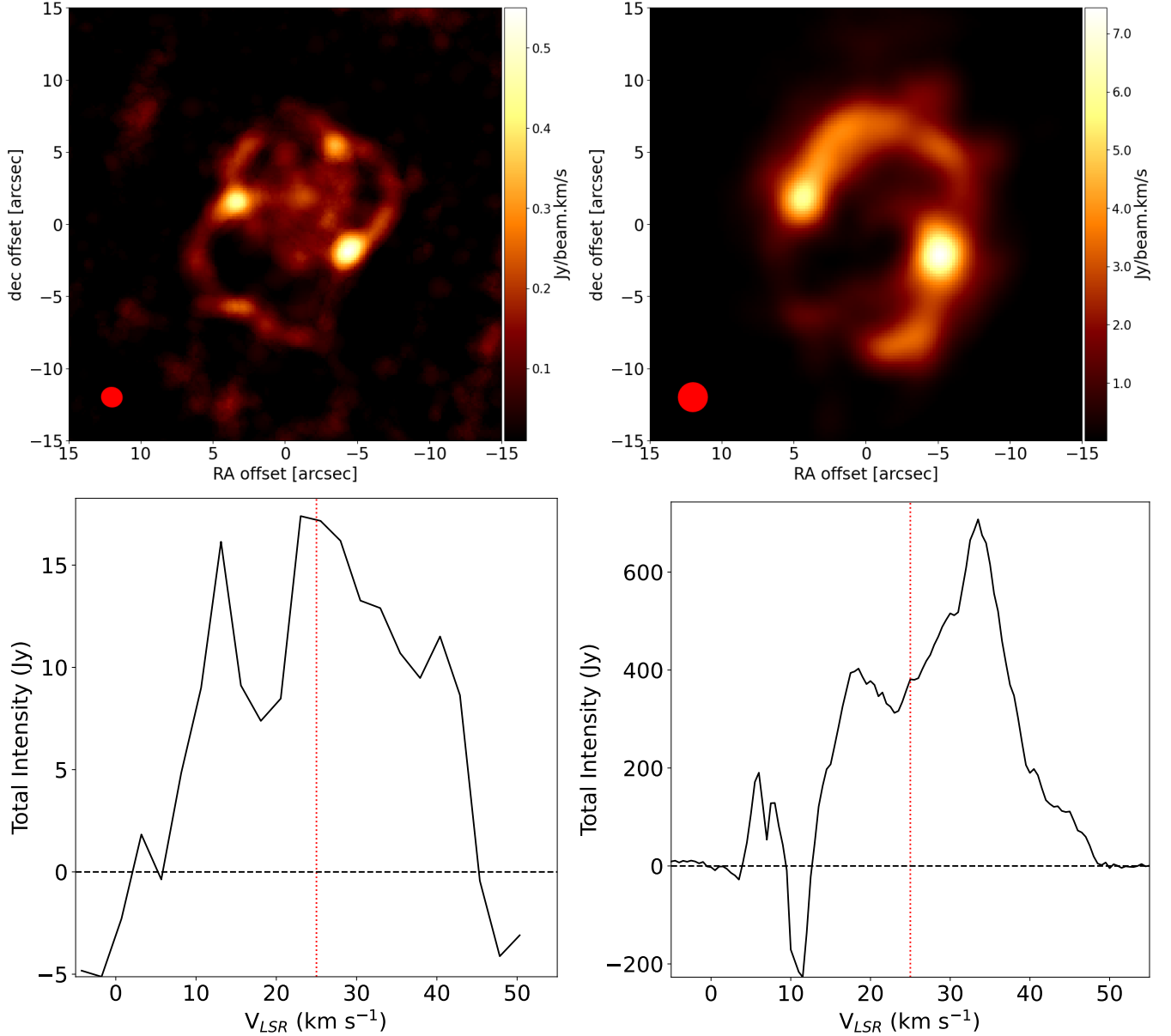


Figure 4. *Top:* CO⁺(2-1) (left) and HCO⁺(1-0) (right) emission integrated over the full range of channels that display signal (0.7–47.8 km s⁻¹ for CO⁺, 4.5–50 km s⁻¹ for HCO⁺). In each frame, North is up, East is left, and the beams are represented by red ovals in the lower left corners. *Bottom:* Spectra of CO⁺(2-1) (left) and HCO⁺(1-0) (right) emission, obtained as the spatially integrated intensities in the channel maps. The systemic velocity of NGC 7027 ($V_{LSR} = 24.3$ km s⁻¹) is indicated by the dotted line.

ated shell, with peak emission again appearing along the nebular minor axis and a non-axisymmetric dearth of material along the SE quadrant (Figure 4). The HCO⁺ kinematic signatures are overall similar to those seen in CO⁺, with blue-shifted and red-shifted emission to the northwest and southeast, respectively, but additional structures are apparent at the more extreme blue-shifted and red-shifted velocities; in particular, prominent blue-shifted emission features appear in the northern regions of the nebula.

The line profile of HCO⁺ extracted from velocity channels (Figure 4, lower right) displays a broad pedestal of emission over the range ~ 5 –50 km s⁻¹ interrupted by a deep, narrow absorption feature at ~ 10 –13 km s⁻¹. In the HCO⁺ channel maps (Figure 3, upper left), the absorption is indeed most clearly seen in the 10.5 and 13.0 km s⁻¹ frames, with a depth of ~ -0.4 Jy beam⁻¹ compared to the continuum-subtracted baseline. Previous emission line surveys have identified blue-shifted absorption and proposed that a cold obscuring

layer of HCO^+ gas is responsible (Deguchi et al. 1990; Bublitz et al. 2019). Figure 3 marks the first interferometric map of such a region in NGC 7027, and demonstrates that the region of absorption appears as a ring-like feature cospatial with that of the continuum emission in the nebula (Figure 5, top right). This suggests that the blue-shifted HCO^+ absorption feature is formed by a layer of cold molecular gas in front of the continuum source, which is presumably free-free radiation from a dense shell of photoionized gas. Furthermore, we speculate that this layer of cold HCO^+ is at least moderately opaque for the absorption feature to be present.

4. ANALYSIS AND DISCUSSION

Figure 5 presents a comparison of the spatial structure of velocity-integrated CO^+ and HCO^+ emission with the 1.3 mm NOEMA continuum image, in addition to the archival HST/NICMOS near-IR H_2 image and SMA $\text{CO}(3-2)$ map. The left column compares the velocity-integrated CO^+ map with contours of continuum emission and H_2 , as well as an overlay of CO^+ contours onto CO . The right column overlays contours of HCO^+ with the continuum, CO^+ , and CO . In Figure 6 we display linear cuts through the moment 0 maps, along the nebula’s major and minor axes ($P.A. = -25^\circ$ and 65° , respectively), through the images of CO^+ and HCO^+ , as well as through the H_2 and the 1.3 mm continuum images. The linear cuts have been fitted with multiple Gaussian functions, to facilitate comparisons of the positions of emission peaks along the major and minor axes. The discussions that follow in Sections 4.1 and 4.2 for CO^+ and HCO^+ , respectively, are derived from the analysis presented in Figs. 5 and 6. Section 4.3 presents a kinematic analysis of the HCO^+ data.

4.1. CO^+

Comparison of the NOEMA CO^+ image with that of the cleaned HST/NICMOS H_2 image reveals highly cospatial emission, in which both the ionized and neutral molecular gas trace the multi-lobed, pillow-like structure of NGC 7027 (Figure 5, middle left). A prominent torus of material is present along the equatorial plane, with the brightest emission occurring at the two edges of the equatorial region. These intensity hot-spots also appear in the H_2 map, with the Eastern edge occurring marginally interior to CO^+ . Similar emission peaks are detected at the NW and SE ends of the H_2 lobes, also coincident with CO^+ emission peaks. In contrast, the CO^+ and CO emission morphologies are strikingly different (Figure 5, lower left).

A minor axis cut across the H_2 map (i.e., along the nebula’s equatorial plane) reveals a pair of emission

peaks at the edges of the waist (Figure 6). Although the Eastern-most feature appears offset from the minor axis, it and its opposite component appear at $4.29''$ and $-4.24''$ offset from the CSPN, while the inner bright components of the waist lie at $3.32''$ and $-2.88''$. CO^+ displays somewhat narrower emission peaks along the minor axis at $\pm 4.20''$ offsets, roughly aligning with the two outer H_2 peaks. The inner H_2 peaks do not have an apparent CO^+ counterpart, indicating CO^+ lies closer to the adjacent molecular rich regions. The emission along the major axis is similarly cospatial, with the outermost CO^+ peaks lying at a N-S average CSPN displacement of $6.4''$ and the outermost H_2 at $6.6''$, well within the respective ($\sim 0.8''$) FWHMs of these local peaks in emission. It is hence apparent that, overall, the CO^+ and H_2 emission are tracing the same emitting region. In contrast, the 1.3 mm continuum emission has an extent of $2.85''$ and $3.53''$ along the nebular minor and major axes, respectively; assuming the continuum emission is due to free-free radiation from dense plasma, this indicates that the densest region of ionized gas lies well inside that of the CO^+ and H_2 emitting region.

As previously noted, $2.12 \mu\text{m}$ H_2 emission can serve as a UV irradiation tracer, and various studies have discussed the likelihood that, in NGC 7027, this H_2 rovibrational line is excited via UV fluorescence and, hence, traces a PDR within the nebula (Graham et al. 1993; Kastner et al. 1996; Latter et al. 2000; Cox et al. 2002). The strong similarity between the CO^+ and H_2 emission surfaces therefore serves as definitive evidence that, Although CO^+ has been flagged as a potential XDR tracer (Wolfire et al. 2022), NGC 7027 appears to be a clear case where CO^+ traces the PDR. Comparable results were found in Mon R2, where CO^+ resides at the atomic-molecular interface of the star-forming region (Treviño-Morales et al. 2016). In that study, the spatial coincidence of CO^+ with PAHs and $[\text{C II}]$, which typically lie along the fluorescent H_2 emission region of PDRs, demonstrated that the CO^+ is UV-enhanced, via reactions with OH or perhaps CO charge transfer. Given the C-rich nature of NGC 7027, a sequence consisting of UV-driven H_2 photodissociation and subsequent photoionization of H, followed by charge transfer with CO, may be driving the formation of CO^+ in its PDR layer.

4.2. HCO^+

In comparing the HCO^+ total intensity map with that of CO^+ (Figure 5, middle right), it is readily apparent that the emission morphologies of the two species diverge significantly. Minimal HCO^+ is present along the line of sight within the central cavity of NGC 7027, and the HCO^+ emission peaks, as well as the extended

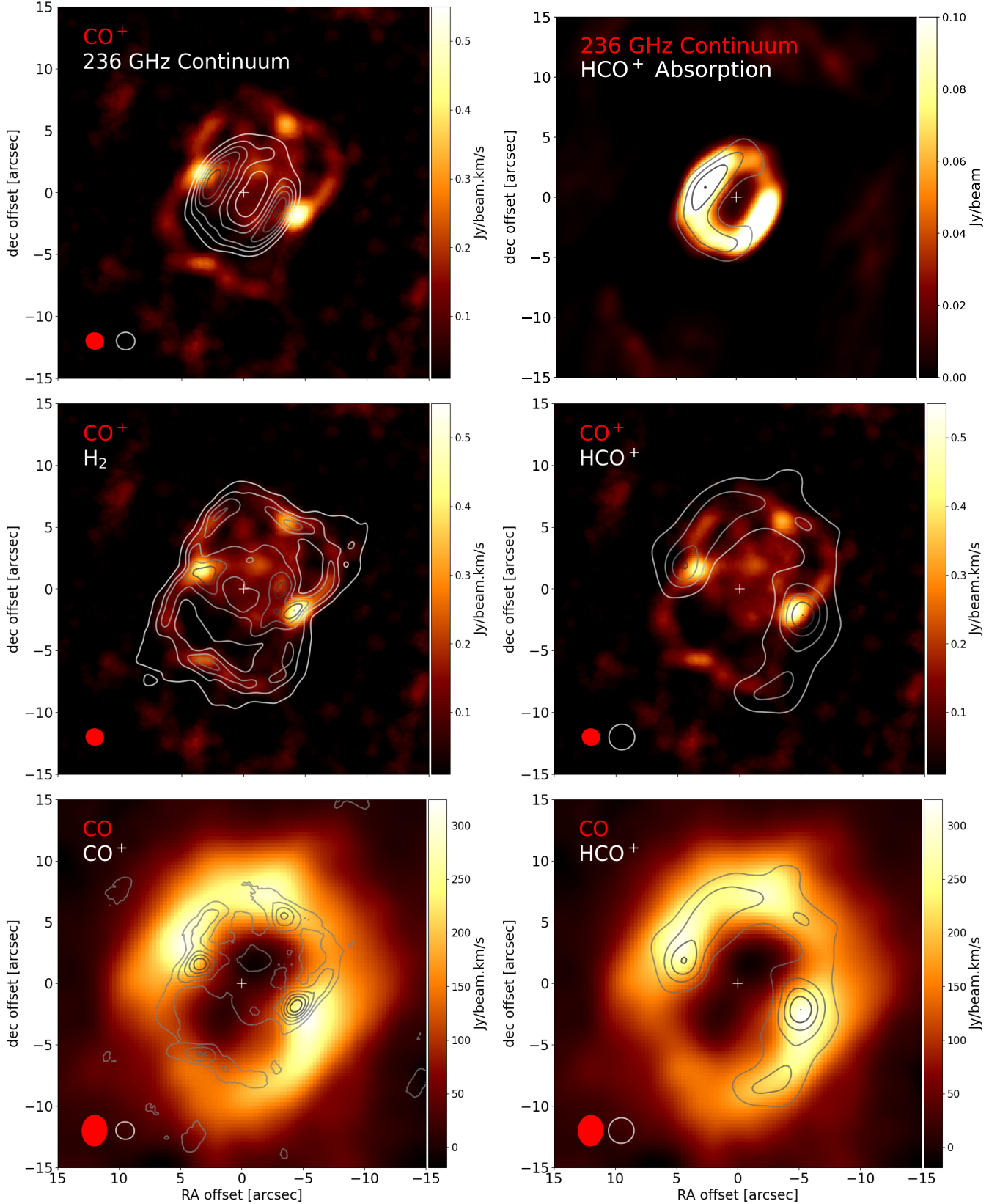


Figure 5. *Top Left:* Contours of the 236 GHz continuum emission from NGC 7027 [0.02, 0.05, 0.08, 0.11, 0.14, 0.17, 0.20 Jy beam⁻¹] overlaid on a velocity-integrated CO⁺ image. *Top Right:* Continuum extracted from off-channel lines in CO⁺ observations. Overlaid contours denote the absorption feature seen from 8.5–13.5 km/s in the velocity averaged image of HCO⁺ [−0.2, −0.15, −0.10, −0.5 Jy beam⁻¹ km s⁻¹]. *Middle:* Molecular map of CO⁺ overlaid with contours of H₂ (left, smoothed to the CO⁺ beamsize) [0.00, 2.24, 4.48, 6.72, 8.96, 11.20 Jy beam⁻¹ km s⁻¹] and of HCO⁺ (right) [0.00, 1.49, 2.98, 4.46, 5.95, 7.44 Jy beam⁻¹ km s⁻¹]. *Bottom:* SMA CO (J=3–2) image of NGC 7027 (Patel et al., in preparation) overlaid with contours of CO⁺ (left) [0.08 0.16 0.24 0.32 0.4 0.48 0.56 Jy beam⁻¹ km s⁻¹] and HCO⁺ (right, same as contours above). Beam sizes for color plots (filled red) and contours (white outline) are included in the lower left of each image.

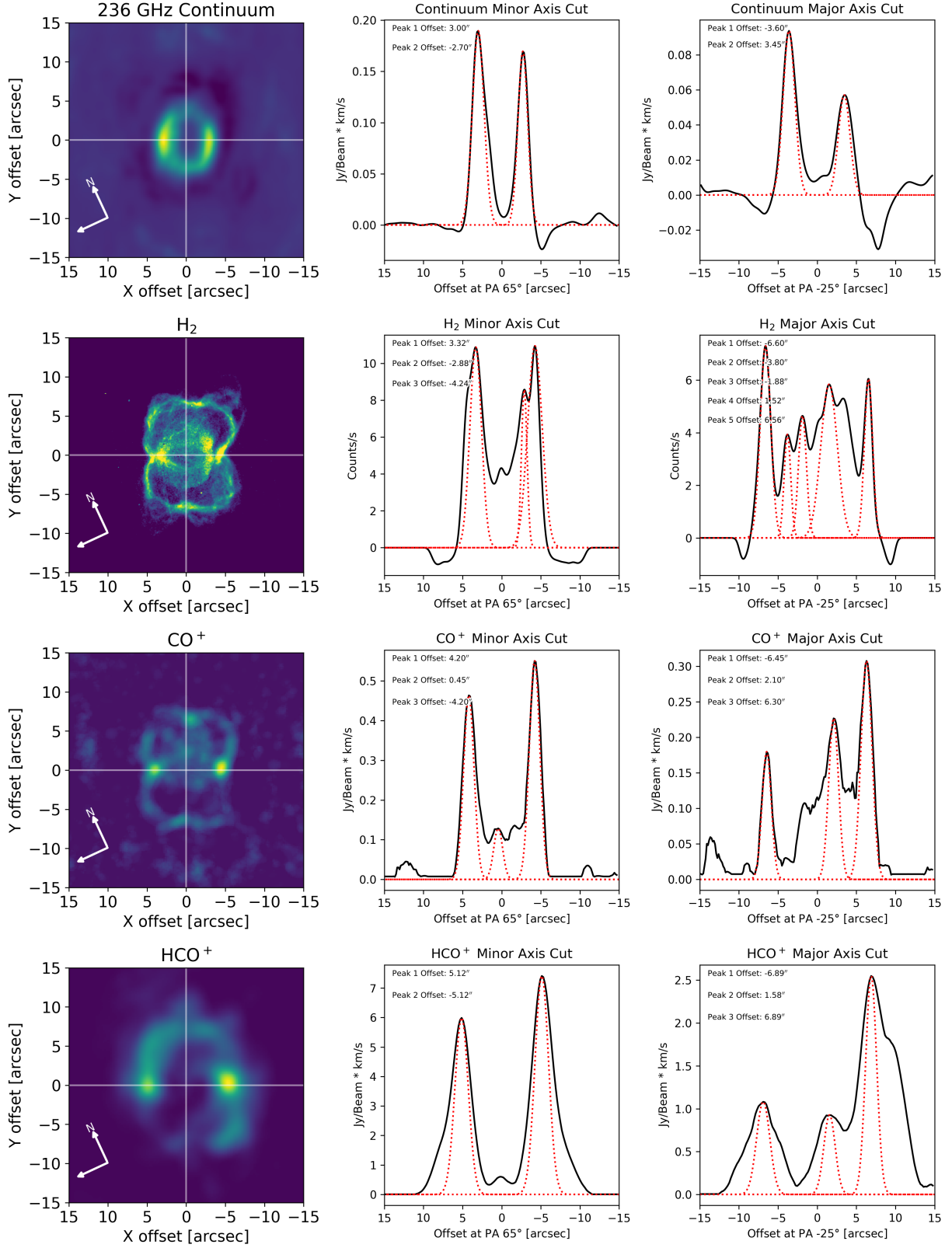


Figure 6. HST/NICMOS and NOEMA images of NGC 7027 with nebula major and minor axes marked in white (left column). Images are rotated -25° with respect to their sky orientation to vertically align the major axis. N is marked in each figure. Intensity of emission along the axes are plotted on the right, with points of greatest emission marked by Gaussian fits in red. Offsets of these peaks in arcseconds from the center of the nebula are displayed in the upper left corner.

HCO⁺ emission structure, lie significantly outside the CO⁺ emission region. The linear cuts in Figure 6 clearly illustrate the displacement of HCO⁺ outside CO⁺ along both the minor and major axes. Specifically, the bright HCO⁺ peaks along the nebular waist lie $\sim 0.9''$ outside their CO⁺ counterparts, while the brightest HCO⁺ emission along the major axis lies $\sim 0.5''$ outside that of CO⁺. It is also evident that detectable HCO⁺ extends well beyond the outer CO⁺ emission boundary.

Furthermore, in stark contrast to the general lack of correspondence of CO⁺ and CO emission (Figure 5, bottom left), HCO⁺ closely follows the overall CO emission morphology (Figure 5, bottom right). Emission from both molecules is similarly extended, with peak intensities near the nebular waist and weaker emission along a P.A. of 60° (i.e., towards the SE quadrant) as well as toward the NW.

The foregoing strongly suggests that the HCO⁺ abundance peaks in the extended molecular envelope of NGC 7027, well outside the region of peak CO⁺ production. This in turn suggests that HCO⁺ production proceeds through X-ray ionization of molecular gas in an XDR that lies outside of the PDR traced by CO⁺ (and near-IR H₂). It remains to determine, via modeling, whether the source of X-ray ionization is the luminous, extended X-ray emission imaged by Chandra (Montez & Kastner 2018), NGC 7027’s exceedingly hot and luminous central star (Moraga et al. 2022), or some combination of the two. Regardless, production of HCO⁺ via dissociative recombination of CO⁺ in the nebula’s PDR appears to be ruled out by these NOEMA observations.

4.3. Multipolar Jets Traced by HCO⁺

We consider here whether and how the CO⁺ and (in particular) HCO⁺ emission from NGC 7027 traces the complex system of outflows that appear to be impinging on and puncturing the inner, elliptical shell of ionized gas (seen in the 1.3 mm continuum image) as well as the nebula’s outer dust ring system (see Moraga et al. 2022).

Cox et al. (2002) first raised the possibility of such a system of fast outflows in NGC 7027. They identified a number of cavities or breakouts, in the form of holes in their velocity-integrated near-IR H₂ emission map, which they attributed to multiple point-symmetric outflows that have pierced the otherwise conical bipolar shell that surrounds NGC 7027’s ionized core. Tracing back from the holes suggests three sets of oppositely directed, narrow, collimated outflows (jets) emanating

from the CSPN (hereafter Outflows 1, 2, and 3⁴) have broken through the H₂ shell at some point in the nebula’s recent history. This interpretation is supported by subsequent modeling of CO emission-line interferometry by Nakashima et al. (2010), who estimated position angles of -53° , 4° , and -28° and inclinations (with respect to the plane of the sky) of 55° , 35° , and -25° , respectively, for Outflows 1, 2, and 3.

As described in § 4.1, the velocity-integrated CO⁺ map bears strong resemblance to the near-IR H₂ image — including the precise positions of emission deficits and peaks — such that the same (three) collimated outflow punctures seen in velocity-integrated H₂ are also present in velocity-integrated CO⁺ (compare our Figure 4 with Figure 10 in Cox et al. 2002). Furthermore, comparison of our Figure 2 with Figure 6 in Cox et al. (2002) demonstrates that the CO⁺ kinematics closely match those of H₂.

Given emission from HCO⁺ closely traces that of CO (Figure 5), we might expect to see similar evidence for the presence of multiple jets associated with the outflows, in the form of spatially localized high-velocity HCO⁺ emission (as described by Nakashima et al. 2010, in the case of CO). Indeed, we have isolated three distinct regions of blue-shifted emission at $\sim 15\text{--}21\text{ km s}^{-1}$ from the nebular systemic velocity, two of which have red-shifted counterparts at similar velocity offsets (Figure 7). The strongest blue-/red-shifted emission pair lies at P.A. = 6°, along Outflow 2. The next strongest pair, along Outflow 3, lines up well with the major axis of NGC 7027 at P.A. = -25° , but appears inverted with respect to Outflow 2 due to its inclination, with red-shifted emission north of the central star and blue-shifted toward the south. As also discussed in Moraga et al. (2022), this orientation suggests the outflow lies roughly along the plane of the nebular waist. Meanwhile, Outflow 1 only displays weak high-velocity blue-shifted HCO⁺ emission at P.A. = -60° , toward the NW corner of the PN; no red-shifted emission counterpart is detected.

The alignment of high-velocity Br γ emission with Outflow 1 (Cox et al. 2002) points toward it being the most recent occurrence of a processing, episodic outflow. This conclusion is supported by evidence that the strongest shocks lie along this same direction (Moraga et al. 2022). These shocks may be dissociating the molecular gas along the direction of Outflow 1, resulting in weak HCO⁺ (and CO) emission relative to that ob-

⁴ We have adopted the outflow naming convention of Cox et al. (2002), which corresponds to Nakashima et al. (2010) directions A, B, and C as well as to their red, yellow, and blue bicones.

served along Outflows 2 and 3. The mechanism behind the asymmetric shock front, whereby HCO^+ gas in the SE is fully dissociated, yet HCO^+ in the NW remains intact, is as yet unclear.

5. CONCLUSIONS

With a massive molecular envelope that is exposed to intense UV and X-ray irradiation from its central star and associated wind shocks, the young and rapidly evolving PN NGC 7027 provides an unrivaled opportunity to study, and attempt to distinguish between, photon-dominated regions (PDRs) and X-ray-dominated regions (PDRs). In addition, while both CO^+ and HCO^+ are detected in various astrophysical environments, present theory leaves open questions as to how these two molecules form and whether they might serve as probes of PDR versus XDR chemistry. We have used the IRAM NOEMA interferometer to obtain maps of $\text{CO}^+(2-1)$ and $\text{HCO}^+(1-0)$ emission, at $\sim 2''$ resolution, from NGC 7027. The former constitutes the first interferometric map of the molecular ion CO^+ in any astrophysical source. The results reveal that CO^+ and HCO^+ trace fundamentally different nebular environments within NGC 7027. The CO^+ emission is precisely cospatial with near-IR H_2 emission, hence effectively tracing the inner boundaries of the PDR, where CSPN UV radiation drives the chemistry. In contrast, HCO^+ and neutral CO emission display similar morphologies, and comparison of the limb-brightened edges of the CO^+ and HCO^+ maps reveals a systematic radial offset, wherein regions of brightest HCO^+ lie $\sim 1''$ (~ 900 au) outside of the corresponding CO^+ emission peaks. This indicates that HCO^+ is enhanced by dust-penetrating soft X-rays in an XDR that surrounds the PDR. High-velocity HCO^+ emission is also found to trace at least three distinct outflows from the central star at position angles of 6° , -25° , and -60° , providing additional evidence that a rotating, episodic jet has re-

peatedly pierced the PDR in NGC 7027's short lifetime, generating X-ray-induced HCO^+ and, in the case of the most recent outflow (oriented SE-NW), fully dissociating shocks. The comparison of interferometric CO^+ and HCO^+ maps of NGC 7027, in conjunction with near-IR H_2 and radio CO observations, thus serves to disentangle and spatially delineate the UV- and X-ray-induced PDR and XDR molecular environments within NGC 7027.

1 This work is based on observations carried out under
 2 projects W16BH and W17AV with the IRAM NOEMA
 3 Interferometer. IRAM is supported by INSU/CNRS
 4 (France), MPG (Germany) and IGN (Spain). We thank
 5 Michael Bremer (IRAM) for reduction of the NOEMA
 6 CO^+ data, and Charlène Lefèvre for support in the re-
 7 duction procedure of the HCO^+ data. The Submillimeter
 8 Array is a joint project between the Smithsonian
 9 Astrophysical Observatory and the Academia Sinica In-
 10 stitute of Astronomy and Astrophysics and is funded by
 11 the Smithsonian Institution and the Academia Sinica.
 12 J.H.K. acknowledges the support of National Science
 13 Foundation grant AST-2206033 to Rochester Institute
 14 of Technology. M.S.G., J.A., and V.B. are partially
 15 supported by the research grant Nebulaeweb/eVeNts
 16 (PID2019-105203GB-C21) of the Spanish AEI (MICIN).
 17 I.A. acknowledges the support of CNPq, Conselho Na-
 18 cional de Desenvolvimento Científico e Tecnológico -
 19 Brazil, process number 157806/2015-4 and the Coor-
 20 denação de Aperfeiçoamento de Pessoal de Nível Supe-
 21 rior - Brasil (CAPES) - Finance Code 001. The authors
 22 wish to thank Alex Wickham-Pirowski for initial devel-
 23 opment of NGC 7027 image rotation and intensity pro-
 24 file code, as well as the anonymous referee for helpful
 25 comments that improved the clarity of this paper.

Facilities: NOEMA, SMA, HST

REFERENCES

- Ali, A., Ismail, H. A., & Alsolami, Z. 2015, *Astrophysics Space Science*, 357, 21
- Bell, T. A., Whyatt, W., Viti, S., & Redman, M. P. 2007, *Monthly Notices of the Royal Astronomical Society*, 382, 1139
- Bieging, J. H., Wilner, D., & Thronson, Harley A., J. 1991, *ApJ*, 379, 271, doi: [10.1086/170501](https://doi.org/10.1086/170501)
- Bublitz, J., Kastner, J. H., Santander-García, M., et al. 2019, *Astronomy & Astrophysics*, 625, A101
- Cox, P., Huggins, P., Maillard, J.-P., et al. 2002, *Astronomy & Astrophysics*, 384, 603
- Deguchi, S., Izumiura, H., Kaifu, N., et al. 1990, *The Astrophysical Journal*, 351, 522
- Deguchi, S., Izumiura, H., Nguyen-Q-Rieu, et al. 1992, *The Astrophysical Journal*, 392, 597
- Fong, D., Meixner, M., Sutton, E. C., Zalucha, A., & Welch, W. J. 2006, *ApJ*, 652, 1626, doi: [10.1086/508127](https://doi.org/10.1086/508127)
- Graham, J. R., Serabyn, E., Herbst, T. M., et al. 1993, *The Astronomical Journal*, 105, 250
- Güsten, R., Wiesemeyer, H., Neufeld, D., et al. 2019, *Nature*, 568, 357, doi: [10.1038/s41586-019-1090-x](https://doi.org/10.1038/s41586-019-1090-x)

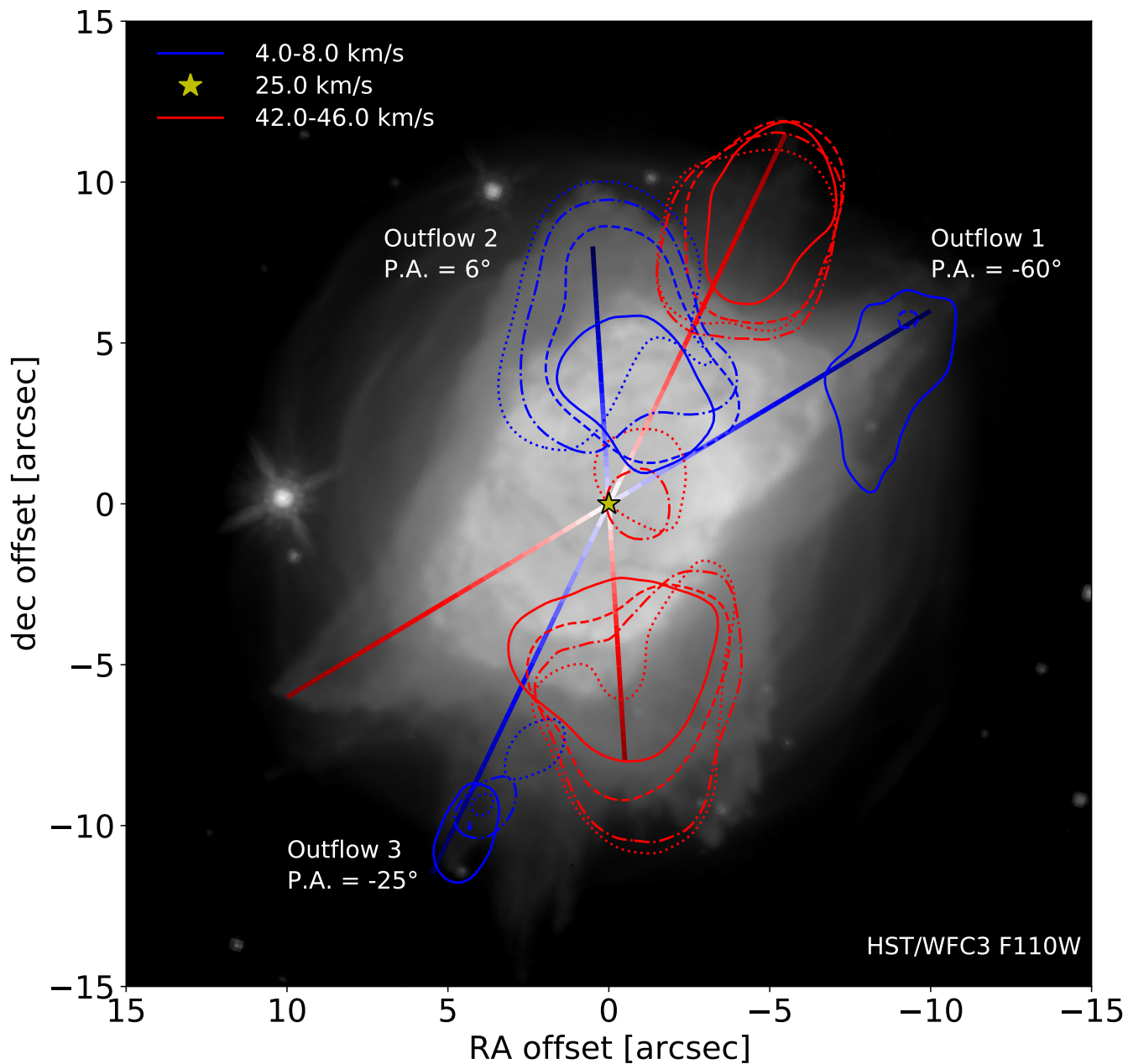


Figure 7. *Left:* WFC3 F110W filter image of NGC 7027 with 15% peak intensity contour overlays from HCO⁺ of the 4–10 km s⁻¹ velocity channels (blue-shifted) and 40–46 km s⁻¹ velocity channels (red-shifted) expanding from the central velocity at 25 km s⁻¹. The HCO⁺ emission traces the fast outflows from the CSPN and their orientation in the sky. Solid contours represent greatest velocity shift, while dashed, dash-dotted, and dotted contours denote velocities closer to the systemic velocity. Solid lines along position angles of 6°, -25°, and -60° represent the approximate length and red- or blue-shifted orientation of the HCO⁺ gas.

- Huang, Z.-Y., Hasegawa, T. I., Dinh-V-Trung, et al. 2010, *The Astrophysical Journal*, 722, 273
- Kastner, J. H., Montez Jr., R., Balick, B., et al. 2012, *The Astronomical Journal*, 144, 58
- Kastner, J. H., Weintraub, D. A., Gatley, I., Merrill, K. M., & Probst, R. G. 1996, *The Astrophysical Journal*, 462, 777
- Kastner, J. H., & Wilson, E. 2021, *ApJ*, 922, 24, doi: [10.3847/1538-4357/ac1f2e](https://doi.org/10.3847/1538-4357/ac1f2e)
- Kimura, R. K., Gruenwald, R., & Aleman, I. 2012, *Astronomy & Astrophysics*, 541, A112
- Latter, W. B., Dayal, A., Biegging, J. H., et al. 2000, *The Astrophysical Journal*, 539, 783
- Latter, W. B., Walker, C. K., & Maloney, P. R. 1993, *The Astrophysical Journal*, 419, L97
- Likkel, L. 1992, *ApJL*, 397, L115, doi: [10.1086/186558](https://doi.org/10.1086/186558)
- Masson, C. R. 1989, *The Astrophysical Journal*, 336, 294
- Montez, Rodolfo, J., & Kastner, J. H. 2018, *The Astrophysical Journal*, 861, 45, doi: [10.3847/1538-4357/aac5df](https://doi.org/10.3847/1538-4357/aac5df)
- Moraga, P., Kastner, J. H., Balick, B., Montez, Jr., R., & Bublitz, J. 2022, *ApJ*, submitted
- Mufson, S. L., Lyon, J., & Marionni, P. A. 1975, *The Astrophysical Journal*, 201, L85
- Nakashima, J.-I., Kwok, S., Zhang, Y., & Koning, N. 2010, *The Astronomical Journal*, 140, 490
- Primiani, R. A., Young, K. H., Young, A., et al. 2016, *Journal of Astronomical Instrumentation*, 5, 1641006, doi: [10.1142/S2251171716410063](https://doi.org/10.1142/S2251171716410063)
- Schmidt, D. R., & Ziurys, L. 2016, *The Astrophysical Journal*, 817, 175
- . 2017, *The Astrophysical Journal*, 835, 79
- Schönberner, D., Balick, B., & Jacob, R. 2018, *Astronomy & Astrophysics*, 609, A216
- Spaans, M., & Meijerink, R. 2007, *The Astrophysical Journal*, 664, L23
- Stäuber, P., & Bruderer, S. 2009, *Astronomy & Astrophysics*, 505, 195
- Treviño-Morales, S. P., Fuente, A., Sánchez-Monge, A., et al. 2016, *Astronomy & Astrophysics*, 593, L12
- Wolfire, M. G., Vallini, L., & Chevance, M. 2022, *ARA&A*, 60, 247, doi: [10.1146/annurev-astro-052920-010254](https://doi.org/10.1146/annurev-astro-052920-010254)
- Zhang, Y., Kwok, S., & Dinh-V-Trung. 2008, *The Astrophysical Journal*, 678, 328
- Zhang, Y., Liu, X.-W., Luo, S.-G., Péquignot, D., & Barlow, M. J. 2005, *Astronomy & Astrophysics*, 442, 249